

# Bayesian Network–Response Regression

**Lu Wang**

*Department of Statistical Science  
Duke University  
Durham, NC 27708-0251, USA*

RL.WANG@DUKE.EDU

**Daniele Durante**

*Department of Statistical Sciences  
University of Padua  
Padua, Italy*

DURANTE@STAT.UNIPD.IT

**David B. Dunson**

*Department of Statistical Science  
Duke University  
Durham, NC 27708-0251, USA*

DUNSON@DUKE.EDU

**Editor:**

## Abstract

There is an increasing interest in learning how human brain networks vary with continuous traits (e.g., personality, cognitive abilities, neurological disorders), but flexible procedures to accomplish this goal are limited. We develop a Bayesian semiparametric model, which combines low-rank factorizations and Gaussian process priors to allow flexible shifts of the conditional expectation for a network-valued random variable across the feature space, while including subject-specific random effects to improve prediction. The formulation leads to an efficient Gibbs sampler along with simple procedures for inference, prediction and goodness-of-fit assessments. The model is applied to learn changes in the brain network with intelligence scores. Results provide interesting insights on the association between intelligence and brain connectivity, while demonstrating improved performance in edge prediction and uncertainty quantification.

## 1. Introduction

We are motivated by recent advances in imaging of structural interconnections among anatomical regions in the human brain. We would like to learn how the brain structural connection networks (connectomes) vary across individuals, and the extent to which such variability is associated with differences in human cognitive traits.

In our motivating application, brain networks are estimated exploiting structural magnetic resonance imaging (MRI) and diffusion tensor imaging (DTI), to obtain a  $V \times V$  symmetric adjacency matrix  $A_i$  for each subject  $i = 1, \dots, n$ . Each cell  $[v, u]$  in the matrix corresponds to a pair of brain regions and  $A_{i[vu]} = A_{i[uv]} = 1$  if there are fibers connecting brain regions  $v$  and  $u$  in individual  $i$ , and  $A_{i[vu]} = A_{i[uv]} = 0$  otherwise. There are  $V = 68$  anatomical regions in our study [Desikan et al. \(2006\)](#) equally divided in the left and right hemisphere. Refer to Figure 1 for an example of the available data.

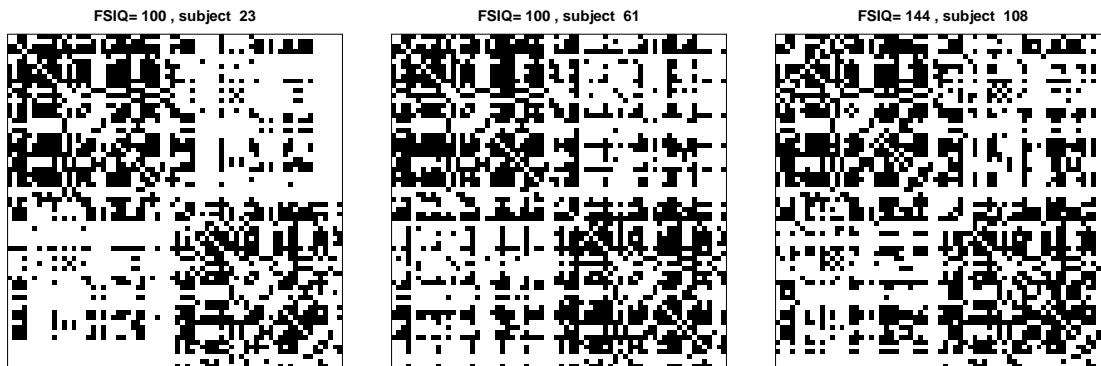


Figure 1: Adjacency matrices for three subjects. Black cell denotes presence of a connection; white cell denotes no connection. FSIQ is an IQ score.

There has been an increasing focus on using brain imaging to better understand the neural pathways underlying human traits, ranging from personality to cognitive abilities to neuropsychiatric disorders (Stam, 2014). Our aim is to develop flexible procedures to improve understanding of how the brain structural connectivity architecture varies in relation to a trait of interest  $x_i \in \mathbb{R}$  measured for each individual  $i = 1, \dots, n$ . In our motivating application, this trait  $x_i$  represents a measure of intelligence for subject  $i$  available via the FSIQ (full scale intelligence quotient) score (Jung et al., 2010).

Network data are challenging to analyze as they require dimensionality reduction procedures to deal with the high number of dyads as well as careful formulations to account for the topological structures of the network. There is a wide literature addressing these goals for a single network. Notable examples include exponential random graph models Holland and Leinhardt (1981); Frank and Strauss (1986) and factorizations, such as stochastic block models Nowicki and Snijders (2001), mixed membership stochastic block models Airoldi et al. (2008) and latent space models Hoff et al. (2002). Although these procedures reduce dimensionality while accounting for specific topological properties, their focus is on a single network instead of multiple network observations collected for different individuals having different attributes.

When interest is in the relationship between the brain structural connection network and a trait of the individual whose brain is being measured, one possibility is to vectorize each adjacency matrix and enter this feature vector in a generalized linear model (GLM) with the trait of interest as the response. However, this procedure does not exploit the network structure of the data and the vector of features arising from a  $68 \times 68$  symmetric adjacency matrix has length  $V(V - 1)/2 = 2278$  which is much larger than the sample size. We have attempted to apply a wide variety of methods for regression with high-dimensional features, and have obtained very poor predictive performance. An alternative is to extract summary statistics for each network – e.g. number of connections, average path length, clustering coefficient – and enter these as features in the regression (Rubinov and Sporns, 2010). However, it is not clear how to best choose such measures and they may fail to capture the relevant characteristics of the network. To overcome these issues, tensor regression models

have been recently developed to characterize the relationship between a scalar response and array-type (tensor) covariate [Zhou et al. \(2013\)](#); [Hoff \(2014\)](#).

We instead view the brain network or graph as a type of ‘object’ response variable in a flexible regression model. This type of network-response regression is applicable in general settings, but there are currently no relevant methods in the literature. Our concrete focus is inference on global and local variations in brain architecture with human traits. We develop a Bayesian semiparametric regression model that reduces dimensionality and efficiently exploits network information via a flexible latent space representation of the brain network, with the latent coordinates of the nodes varying both systematically – according to a trait of the individual, such as IQ – and randomly – due to unmeasured traits and measurement errors – across individuals.

The paper is organized as follows. In Section 2 we describe the model formulation. Section 3 provides details on prior specification and posterior computation. In Section 4, our model is applied to learn changes in the brain network according to intelligence scores, showing improved results in edge prediction, uncertainty quantification and inference.

## 2. Network–Response Regression

Let  $A_i$  denote the adjacency matrix characterizing the undirected brain network with no self-relationships of subject  $i$  and  $x_i$  her feature value, for each  $i = 1, \dots, n$ . As self-relationships are not of interest and  $A_i$  is symmetric, we model  $A_1, \dots, A_n$  by defining a probabilistic generative mechanism for data  $\mathcal{L}(A_1), \dots, \mathcal{L}(A_n)$ , with  $\mathcal{L}(A_i) = (A_{i[21]}, A_{i[31]}, \dots, A_{i[V1]}, A_{i[32]}, \dots, A_{i[V(V-1)]})'$  the vector encoding the lower triangular elements of  $A_i$ , which uniquely characterize the network as  $A_{i[vu]} = A_{i[uv]}$  for every  $v = 2, \dots, V$ ,  $u = 1, \dots, v-1$  and  $i = 1, \dots, n$ . As a result,  $\mathcal{L}(A_i)$  is a vector of binary elements  $\mathcal{L}(A_i)_l \in \{0, 1\}$ , encoding the presence or absence of an edge among the  $l$ th pair of brain regions in the  $i$ th subject, for each  $l = 1, \dots, V(V-1)/2$  and  $i = 1, \dots, n$ .

Based on the above notation, developing a regression model for a network-valued response translates into statistical modeling of how a vector of binary elements changes across the values of a feature. However, it is important to explicitly account for the special structure of our data. Specifically, networks are potentially characterized by specific underlying patterns – such as transitive relations, community structures and  $k$ -stars – which induce dependence among edges within each brain. As a result, by carefully accommodating the network structure in modeling of  $\mathcal{L}(A_1), \dots, \mathcal{L}(A_n)$ , one might efficiently borrow information within each  $\mathcal{L}(A_i)$  and across the features, while reducing dimensionality and inferring specific network properties along with their changes across features.

In modeling of  $\mathcal{L}(A_1), \dots, \mathcal{L}(A_n)$  we look for a representation which can flexibly characterize variability across individuals in brain structure, while accommodating network structure within each brain and learning changes with a trait of interest. Individual variability [Mueller et al. \(2013\)](#) and specific network structures [Bullmore and Sporns \(2009\)](#) have been shown to substantially affect the functioning of networked brain systems, with these systems often varying with human traits; see [Stam \(2014\)](#) for a study on changes in brain networks across neurological disorders.

Consistently with our goals and letting  $\mathcal{L}(A_i)$  denote the random variable associated to the brain network of subject  $i$ , we characterize individual variability by assuming the edges among

pairs of brain regions in the  $i$ th subject are conditionally independent Bernoulli random variables, given a subject-specific edge probability vector  $\pi^{(i)} = \{\pi_1^{(i)}, \dots, \pi_{V(V-1)/2}^{(i)}\}'$ , with  $\pi_l^{(i)} = \text{pr}\{\mathcal{L}(\mathcal{A}_i)_l = 1\}$ ,

$$\mathcal{L}(\mathcal{A}_i)_l \mid \pi_l^{(i)} \sim \text{Bern}\{\pi_l^{(i)}\}, \quad (1)$$

independently for each  $l = 1, \dots, V(V-1)/2$  and  $i = 1, \dots, n$ . Equation (1) incorporates individual variability, but fails to account for two important sources of information in our data. We expect dependence between edge probabilities in  $\pi^{(i)}$ ,  $i = 1, \dots, n$  due to network topology. Moreover, it is reasonable to expect that brains of subjects with similar traits will have comparable network structure. To account for these additional sources of information, we define the edge probabilities as a function of subject-specific node positions in a latent space, with these positions centered on a higher-level mean which changes with the trait of interest. Specifically, letting  $l$  denote the pair of brain regions  $v$  and  $u$  with  $v > u$ , we first borrow information within each network by assuming

$$\text{logit}\{\pi_l^{(i)}\} = Z_l + \sum_{r=1}^R Y_{vr}^{(i)} Y_{ur}^{(i)}, \quad (2)$$

for each  $l = 1, \dots, V(V-1)/2$  and  $i = 1, \dots, n$ . In (2),  $Z_l \in \mathfrak{R}$  is a similarity measure for the  $l$ th pair of nodes shared among all individuals,  $Y_{vr}^{(i)} \in \mathfrak{R}$  is the  $r$ th coordinate of the brain region  $v$  for individual  $i$  and  $Y_{ur}^{(i)} \in \mathfrak{R}$  is the same quantity for the region  $u$ . According to (2) the probability of a connection between the  $l$ th pair of nodes in individual  $i$  increases with their similarity  $Z_l$  – shared among all individuals – and with the dot-product of the nodes latent positions specific to individual  $i$ .

Factorization (2) allows dimensionality reduction from  $n\{V(V-1)/2\}$  edge probabilities for all the individuals, to  $\{V(V-1)/2 + nVR\}$  parameters – with  $R \ll V$  typically. Moreover, equation (2) recalls an eigen-model formulation Hoff (2009), and can accommodate broad topological properties covering block structures and transitive relations – among others.

### 3. Prior Specification and Posterior Computation

#### 3.1 Prior specification

We choose priors for the shared parameters  $Z_l$ ,  $l = 1, \dots, V(V-1)/2$  and the individual-specific latent coordinates  $Y_{vr}^{(i)}$  for each  $v = 1, \dots, V$ ,  $r = 1, \dots, R$  and  $i = 1, \dots, n$ . The priors are chosen to allow simple posterior computation, favor borrowing of information between different individuals and allow the latent coordinates to smoothly change across the trait values. Subjects having similar traits are expected to have more similar brain networks, and we learn the degree of similarity, which can be close to zero for uninformative traits. We let

$$Z_l \sim \text{N}(\mu_z, \sigma_z^2), \quad (3)$$

independently for  $l = 1, \dots, V(V-1)/2$ <sup>1</sup> and

$$Y_{vr}^{(i)} \sim \text{N}\{\mu_{vr}(x_i), 1\}, \quad (4)$$

---

1. We also attempted t-distribution priors but did not observed improvements in inference and prediction.

independently for each  $v = 1, \dots, V$ ,  $r = 1, \dots, R$  and  $i = 1, \dots, n$ . (3) provides a *baseline* characterization for a typical brain upon which we build in individual-specific deviations. To accommodate systematic deviations, we incorporate mean functions  $\mu_{vr}(\cdot)$  characterizing the change in the  $v$ th brain region and  $r$ th latent dimension with the trait of interest according to (4).

In modeling  $\mu_{vr}(\cdot)$ , we could consider a Gaussian process (GP) prior for each  $v = 1, \dots, V$  and  $r = 1, \dots, R$ . However, as the number of nodes increases, we face scalability issues. To reduce dimensionality, we define each  $\mu_{vr}(\cdot)$  as a linear combination of a smaller number of *dictionary functions*  $W_{kr}(\cdot)$ ,  $k = 1, \dots, K < V$  and  $r = 1, \dots, R$ , obtaining

$$\mu_{vr}(\cdot) = \sum_{k=1}^K G_{vk} W_{kr}(\cdot), \quad (5)$$

for each  $v = 1, \dots, V$  and  $r = 1, \dots, R$ , where  $G_{vk}$ ,  $v = 1, \dots, V$  and  $k = 1, \dots, K$  are coefficients common to all the subjects. Factorization (5) further reduces the number of unknown functions from  $V \times R$  to  $K \times R$ , where  $K$  is typically smaller than  $V$ . Factorizations (2) and (5) are not unique; however, we avoid identifiability constraints as the focus of our inference is not on latent coordinates but on how the overall network structure varies systematically with traits and randomly across individuals. Such inferences can be accomplished via appropriate functionals of the edge probabilities  $\pi^{(i)}$ , as we will illustrate.

In choosing priors for the components in factorization (5), we first let

$$W_{kr}(\cdot) \sim \text{GP}(0, c) \quad (6)$$

independently for each  $k = 1, \dots, K$  and  $r = 1, \dots, R$ , with  $c$  the squared exponential correlation function  $c(x_i, x_j) = \exp\{-\kappa(x_i - x_j)^2\}$ ,  $\kappa > 0$ . To allow adaptive deletion of unnecessary dictionary functions, we incorporate a shrinkage effect in the prior for the coefficients  $G_{vk}$ ,  $v = 1, \dots, V$  and  $k = 1, \dots, K$ , letting

$$G_{vk} \sim \text{N}(0, \tau_k^{-1}), \quad v = 1, \dots, V, \quad k = 1, \dots, K \quad (7)$$

$$\tau_k \sim \text{Ga}(aq^{3(k-1)}, q^{2(k-1)}), \quad q > 1. \quad (8)$$

In (7),  $\tau_k$  provides a global column-wise shrinkage effect on  $G_{vk}$ . High values of  $\tau_k$  force the prior for  $G_{vk}$  to be concentrated around zero *a priori*, deleting the effect of the corresponding dictionary function  $W_{kr}(\cdot)$  in factorization (5). Equation (8) is carefully defined to allow this shrinkage effect to be increasingly strong as  $k$  grows. A graphical representation of our hierarchical model formulation is provided in Figure 2.

### 3.2 Posterior computation

Given priors defined in equations (3)–(8), posterior computation for model (1) with individual-specific edge probabilities factorized as in (2) proceeds via a simple Gibbs sampler leveraging Pólya-Gamma data augmentation (Polson et al., 2013), which allows conjugate inference in Bayesian logistic regression. We summarize below the main steps of the MCMC routine. Step-by-step derivations and guidelines for implementation are provided in the Supplementary Materials.

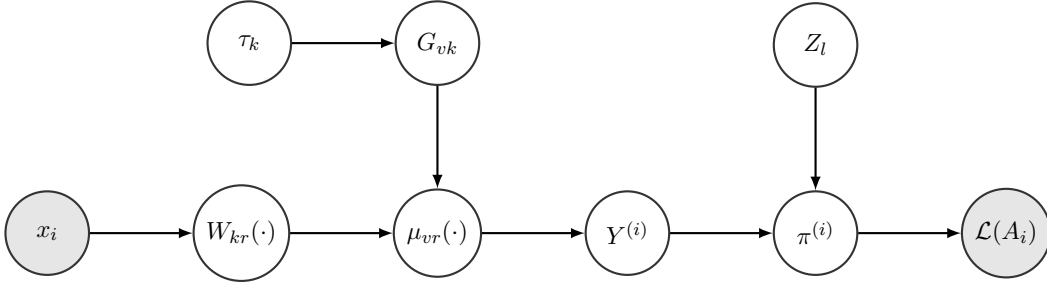


Figure 2: Summarized graphical representation of our hierarchical model. The indices of the quantities in the figure are  $l = 1, \dots, V(V-1)/2$ ,  $v = 1, \dots, V$ ,  $k = 1, \dots, K$ ,  $r = 1, \dots, R$  and  $i = 1, \dots, n$ .

1. Update each augmented data  $\omega_l^{(i)}$ ,  $l = 1, \dots, V(V-1)/2$ ,  $i = 1, \dots, n$ , from its full conditional Pólya-Gamma distribution.
2. Given the data  $\{\mathcal{L}(A_i), x_i\}$ ,  $i = 1, \dots, n$ , the latent coordinates  $Y^{(i)}$ ,  $i = 1, \dots, n$  and augmented data  $\omega_l^{(i)}$ ,  $l = 1, \dots, V(V-1)/2$ ,  $i = 1, \dots, n$ , the full conditional posteriors for  $Z_l$ ,  $l = 1, \dots, V(V-1)/2$  are Gaussian distributions.
3. In updating the subject-specific coordinate matrices  $Y^{(i)}$ , for each  $i = 1, \dots, n$ , we block sample the rows of  $Y^{(i)}$  in turns conditionally on the rest of the matrix and the parameters  $G_{vk}$ ,  $v = 1, \dots, V$ ,  $k = 1, \dots, K$ ,  $W_{kr}(x_i)$ ,  $k = 1, \dots, K$ ,  $r = 1, \dots, R$ . This approach allows rewriting the model (1)–(2) as a Bayesian logistic regression for which the Pólya-Gamma data augmentation scheme guarantees conjugate Gaussian full conditionals.
4. Given the coordinate matrices  $Y^{(i)}$ ,  $i = 1, \dots, n$  and features  $x_i$ ,  $i = 1, \dots, n$ , updating for the parameters  $G_{vk}$ ,  $v = 1, \dots, V$ ,  $k = 1, \dots, K$  and the trajectories  $W_{kr}(\cdot)$ ,  $k = 1, \dots, K$ ,  $r = 1, \dots, R$  at the observed trait values, proceed exploiting the properties of GP priors and standard steps in Bayes multiple linear regression.
5. Conditioned on  $G_{vk}$ ,  $v = 1, \dots, V$ ,  $k = 1, \dots, K$  the shrinkage parameters  $\tau_k$ ,  $k = 1, \dots, K$  are updated from their full conditional Gamma distributions.
6. To obtain the subject-specific edge probabilities  $\pi_l^{(i)}$ ,  $l = 1, \dots, V(V-1)/2$ ,  $i = 1, \dots, n$  simply apply equation (2) to the posterior samples of  $Y^{(i)}$ , for each  $i = 1, \dots, n$  and  $Z_l$ ,  $l = 1, \dots, V(V-1)/2$ .

Our procedure allows inference on the posterior distribution of  $\pi_l^{(i)}$  even if its corresponding edge variable  $\mathcal{L}(A_i)_l$  is missing. This can be accomplished by adding a further data augmentation step imputing the missing edges from their conditional distribution given the current state of the chain:

7. If  $\mathcal{L}(A_i)_l$  is missing, sample this edge from  $\mathcal{L}(A_i)_l \mid \pi_l^{(i)} \sim \text{Bern}\{\pi_l^{(i)}\}$ .

Obtaining posterior samples also for the individual-specific edge probabilities associated to unobserved edges is a key for prediction. Under our Bayesian procedure and recalling

equation (1), prediction of unobserved edges can be obtained exploiting the mean of the posterior predictive distribution

$$\begin{aligned} \mathbb{E}\{\mathcal{L}(\mathcal{A}_i)_l \mid \mathcal{L}(A_1), \dots, \mathcal{L}(A_n)\} &= \mathbb{E}_{\pi_l^{(i)}} \left[ \mathbb{E}\{\mathcal{L}(\mathcal{A}_i)_l \mid \pi_l^{(i)}\} \mid \mathcal{L}(A_1), \dots, \mathcal{L}(A_n) \right], \\ &= \mathbb{E}\{\pi_l^{(i)} \mid \mathcal{L}(A_1), \dots, \mathcal{L}(A_n)\} \end{aligned} \quad (9)$$

for each possible missing pair  $l = 1, \dots, V(V-1)/2$  in individual  $i = 1, \dots, n$ , where the last expectation simply coincides with the posterior mean of  $\pi_l^{(i)}$ . We use standard font  $\mathcal{L}(A)$  to define the observed vectors of edges and italics notation  $\mathcal{L}(\mathcal{A})$  to denote the associated random variable.

#### 4. Brain Networks and Intelligence Scores

We apply our model to the dataset MRN-114 at <http://openconnecto.me/data/public/MR/>, which consists of brain structural connectivity data for 114 subjects along with their cognitive ability measured via FSIQ (full scale intelligence quotient) (Jung et al., 2010). FSIQ ranges from 86 to 144 with 48 unique values. In studying the association between intelligence and brain architecture, previous works focus on detecting the activated regions in the brain involved in cognitive control (Leech et al., 2012) or the relationship between intelligence and topological properties of the brain network (Li et al., 2009). We hope to obtain new insights into the neural pathways underlying human intelligence.

In performing posterior computation, we collected 5,000 MCMC iterations setting  $\kappa = 0.001$ ,  $a = 2$ ,  $q = 2$ ,  $\mu_z = 0$  and  $\sigma_z^2 = 10$ . Trace plots for the edge probabilities suggest convergence is reached after 1,000 burn-in iterations. We additionally thin the chains every 4 samples. As the latent dimensions  $R$  and  $K$  are in general unknown, we perform posterior computation for increasing  $R = K = 1, \dots, 6$  and stop when there is no substantial improvement in out-of-sample edge prediction based on the area under the ROC curve (AUC). In computing the AUC, we randomly select 20% of the edges and hold them out for a randomly chosen 50% of the subjects in the dataset. On these held-out test edges the AUC is computed using the posterior mean of their corresponding edge probabilities estimated from the training data, consistently with the procedure in (9). We repeat the procedure 5 times for each setting and report the average AUC together with the standard deviation in Table 1. According to results in Table 1, the network-response model having  $R = K = 5$  provides a good choice for inference and prediction. It is additionally worth noticing how all the AUCs are very high. The reason is that a wide set of brain connections are easier to predict in being either almost always present or absent in the subjects under study.

In the following subsections we discuss the improved performance of our procedure – considering  $R = K = 5$  – in relation to a competitor under different perspectives, including prediction, uncertainty quantification and goodness-of-fit. These improvements are fundamental in refining inference on how network structures change across a continuous feature.



Table 1: AUC on the test data (20% edges randomly held out for 50% subjects) for varying  $R$  and  $K$ .

R=K=1	R=K=2	R=K=3	R=K=4	R=K=5	R=K=6
0.983±0.001	0.986±0.002	0.988±0.001	0.989±0.001	0.990±0.002	0.989±0.001

Table 2: AUC on test data when holding out the hard-to-predict edges for different proportions of subjects. AUC (50%) denotes the AUC when holding out the hard-to-predict edges for 50% of the subjects.

	AUC (25%)	AUC (50%)	AUC (75%)	AUC (100%)
Network-response Regression	0.828±0.005	0.823±0.003	0.815±0.002	0.728±0.000
Hierarchical Logistic Regression	0.688±0.012	0.680±0.003	0.667±0.005	0.499±0.007

#### 4.1 Edge prediction

Consistently with the above discussion, we assess performance in edge prediction for a more challenging scenario holding out only the hard-to-predict edges having empirical probability<sup>2</sup>  $0.2 < \tilde{\pi}_l < 0.8$ . We compare predictive performance with a hierarchical logistic regression model, which borrows information among the edge-specific regression coefficients. Specifically we let

$$\begin{aligned}
\text{logit}\{\pi_l^{(i)}\} &= z_l + \beta_{1l}x_i + \beta_{2l}x_i^2 \\
(z_l, \beta_{1l}, \beta_{2l})' &\sim N_3(b, B^{-1}) \\
b &\sim N_3(b_0, \Sigma_b), \quad B \sim \text{Wishart}(\nu_0, U_0)
\end{aligned}$$

for  $l = 1, \dots, V(V-1)/2$  with  $b_0 = (0, 0, 0)'$ ,  $\Sigma_b = \text{diag}(10, 10, 10)$ ,  $\nu_0 = 5$  and  $U_0 = I_3$ .

Table 2 compares performance for the out-of-sample prediction task, when holding out the hard-to-predict edges for an increasing proportion of randomly selected subjects. Also in this case we repeat the procedure 5 times for each setting and report the average AUC together with the standard deviation. Results in Table 2 confirm that our approach has substantial advantages over usual hierarchical modeling, likely due to the careful modeling of individual variability in network structure, while borrowing information within each network and across subjects.

#### 4.2 Uncertainty quantification and probability calibration

One important advantage of a flexible Bayesian approach over methods relying on optimization or simplified hierarchical modeling is the ability to accurately characterize uncertainty in learning how brain structure varies over individuals, systematically in relation to traits and randomly due to unmeasured factors and measurement errors.

We assess performance in uncertainty quantification by evaluating probability calibration in the prediction task, focusing again on the hard-to-predict edges, held out for 50% of the

2. The empirical edge probability  $\tilde{\pi}_l$  is defined as  $\tilde{\pi}_l = \sum_{i=1}^n \mathcal{L}(A_i)_l / n$  for each  $l = 1, 2, \dots, V(V-1)/2$ .



Table 3: Proportion of actual edges among those predicted to have an edge with probability within each bin.

Bins	[0, 0.1]	(0.1, 0.2]	(0.2, 0.3]	(0.3, 0.4]	(0.4, 0.5]
Network-response Regression	0.0651	0.1448	0.2265	0.3330	0.4197
Hierarchical Logistic Regression	0.2880	0.2422	0.2697	0.3454	0.4436
Bins	(0.5, 0.6]	(0.6, 0.7]	(0.7, 0.8]	(0.8, 0.9]	(0.9, 1]
Network-response Regression	0.5093	0.6269	0.6926	0.7894	0.9132
Hierarchical Logistic Regression	0.5232	0.6151	0.6901	0.7095	0.7404

subjects. We bin the posterior mean of the probabilities for the held out edges in intervals  $[0, 0.1], (0.1, 0.2], \dots, (0.9, 1]$  and – within each bin – we calculate the proportion of actual edges among those predicted to have an edge probability within that bin. If the values of these empirical proportions are actually within the bins they refer to, the procedure is well calibrated and is expected to properly quantify uncertainty.

According to Table 3 our model has good performance in uncertainty quantification, improving probability calibration compared to hierarchical logistic regression.

### 4.3 Goodness-of-fit evaluation

For the subjects comprising the test set in subsection 4.2, we additionally perform posterior predictive checks (Gelman et al., 2014) to assess performance in characterizing key network summary measures – covering network density, average path length, transitivity and hemispheric assortativity – of particular interest in neuroscience (Bullmore and Sporns, 2009). Although the posterior predictive distribution for these summary statistics is not analytically available, it is straightforward to simulate from the posterior predictive distribution exploiting posterior samples of  $\pi_l^{(i)}$  and the assumption  $\mathcal{L}(\mathcal{A}_i)_l \mid \pi_l^{(i)} \sim \text{Bern}\{\pi_l^{(i)}\}$ , for  $l = 1, \dots, V(V-1)/2$  and  $i = 1, \dots, n$ .

Figure 3 compares the network summary measures observed for each subject in the test set with their posterior predictive distribution arising from our network-response model and the hierarchical logistic regression, respectively. The closer the points in Figure 3 are to the diagonal line, the better the model fits the data. Our procedure achieves good performance in characterizing subject-specific key network summary measures, substantially improving over our competitor. This motivates further analyses on how the brain network changes, on average, across FSIQ levels.

### 4.4 Inference on changes in the brain connectivity architecture across FSIQ scores

The cerebrum of the brain is divided into 5 main anatomical lobes: frontal lobe, limbic cortex, occipital lobe, parietal lobe and temporal lobe (Kang et al., 2012). In order to provide interpretable inference on how the network architecture changes across FSIQ we focus on the posterior distribution for the trajectories of aggregated connectivity patterns considering possible combinations of hemispheric and lobe membership of the brain regions. For example,

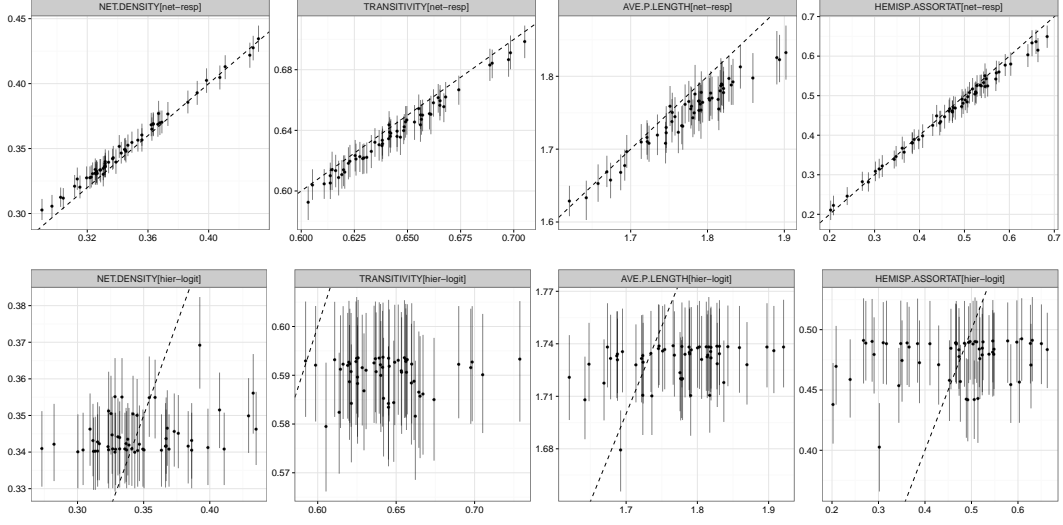


Figure 3: Goodness-of-fit assessment for selected network summary measures under the two different modeling procedures. Upper panels: for network–response regression, plot of the observed network summary measures for each subject in the test set ( $x$ -axis) versus their corresponding mean arising from the posterior predictive distribution ( $y$ -axis). Segments represent the 95% posterior predictive intervals. Lower panels: same quantities from hierarchical logistic regression.

the left plot in Figure 4 displays the posterior distribution of the averaged edge probabilities connecting brain regions in different hemispheres, but belonging both to the frontal lobe.

Left and middle plots in Figure 4 show that the aggregated connectivity pathway linking regions in left and right frontal lobe as well as the one connecting regions in the frontal lobe with those in the limbic cortex, increase with FSIQ. This result is interestingly in line with available findings on the role of the frontal lobe in intelligence (Li et al., 2009). To provide further insights on local changes in the brain architecture with FSIQ, the right plot in Figure 4 highlights the connections whose posterior distributions display the more evident trends with FSIQ. In particular we found all the trajectories for the edges highlighted in the right plot of Figure 4 significantly increase with FSIQ. Consistently with the results in the left plot of Figure 4, almost all these edges connect pairs of brain regions in opposite hemispheres but belonging both to the frontal lobe.

## 5. Conclusion

Motivated by a neuroscience application, we proposed a novel model for flexibly characterizing changes in a network-valued random variable with a continuous trait. The application to learn variations in the brain connectivity architecture across FSIQ shows substantially improved performance in edge prediction, uncertainty quantification, posterior predictive checks and inference.

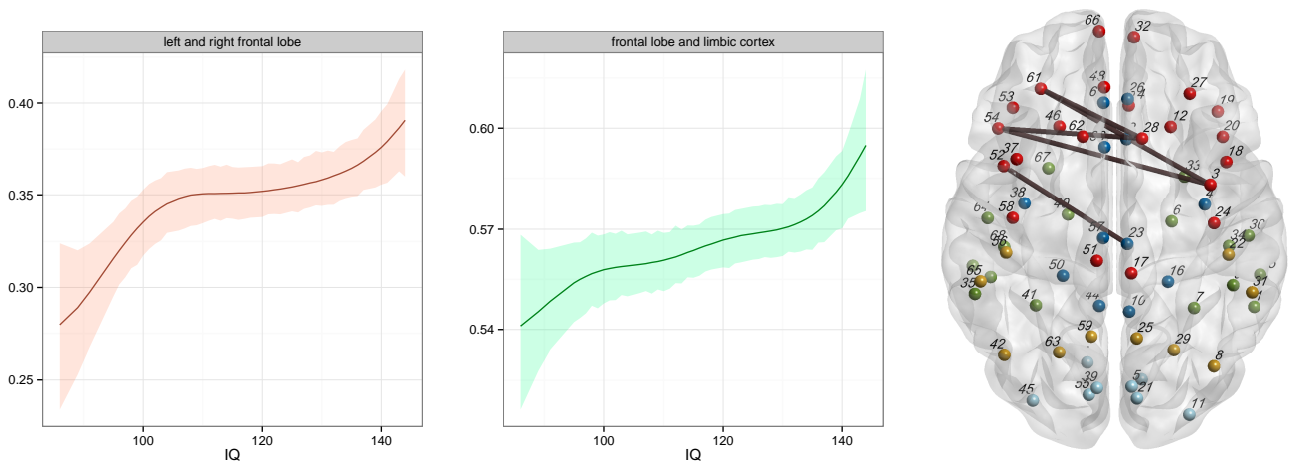


Figure 4: Left plot: average connection probability versus FSIQ for connections linking regions in left and right frontal lobe. Middle plot: average connection probability versus FSIQ for connections linking regions in frontal lobe and limbic lobe. Colored lines denote the point-wise posterior means and colored areas denote the 95% highest posterior density (hpd) intervals from our model. Right plot: 3-D brain network representation showing edges whose trajectories display evident trends across FSIQ based on their posterior distribution. Frontal lobe regions (red), Limbic (dark blue), Parietal (orange), Temporal (olive green), Occipital (light blue).

Although we focus on a single trait, the method is trivially generalized to accommodate multiple traits of an individual. Our procedure has also a broad range of possible applications. Examples include learning changes in co-subscription networks among multiple products for different agencies as a function of profit, or studying how networks of passes in soccer teams change with a measure of team performance – among others. Although our initial results suggest that binary brain networks already contain valuable information about the individual’s brain structure, future research generalizing the proposed model to account for weighted edges, may benefit from the additional information contained in the fiber counts connecting pairs of brain regions.

## References

- Edoardo M. Airoldi, David M. Blei, Stephen E. Fienberg, and Eric P. Xing. Mixed Membership Stochastic Blockmodels. *Journal of Machine Learning Research*, 9:1981–2014, 2008. ISSN 1532-4435.
- Ed Bullmore and Olaf Sporns. Complex brain networks: graph theoretical analysis of structural and functional systems. *Nature Reviews Neuroscience*, 10(3):186–198, 2009.
- Rahul S Desikan, Florent Ségonne, Bruce Fischl, Brian T Quinn, Bradford C Dickerson, Deborah Blacker, Randy L Buckner, Anders M Dale, R Paul Maguire, Bradley T Hyman, Marilyn S Albert, and Ronald J Killiany. An automated labeling system for subdividing the human cerebral cortex on mri scans into gyral based regions of interest. *Neuroimage*, 31(3):968–80, Jul 2006. doi: 10.1016/j.neuroimage.2006.01.021.
- Ove Frank and David Strauss. Markov graphs. *Journal of the American Statistical Association*, 81(395):832–842, Sep 1986. doi: 10.2307/2289017.
- Andrew Gelman, John B Carlin, Hal S Stern, and Donald B Rubin. *Bayesian data analysis*, volume 2. Taylor & Francis, 2014.
- Peter D Hoff. A hierarchical eigenmodel for pooled covariance estimation. *Journal of the Royal Statistical Society: Series B (Statistical Methodology)*, 71(5):971–992, 2009.
- Peter D Hoff. Multilinear tensor regression for longitudinal relational data. *arXiv preprint arXiv:1412.0048*, 2014.
- Peter D Hoff, Adrian E Raftery, and Mark S Handcock. Latent space approaches to social network analysis. *Journal of the American Statistical Association*, 97(460):1090–1098, Dec 2002. doi: 10.1198/016214502388618906.
- Paul W. Holland and Samuel Leinhardt. An exponential family of probability distributions for directed graphs. *Journal of the American Statistical Association*, 76(373):33–50, Mar 1981. doi: 10.2307/2287037.
- Rex E Jung, Judith M Segall, H Jeremy Bockholt, Rane A Flores, Shirley M Smith, Robert S Chavez, and Richard J Haier. Neuroanatomy of creativity. *Human brain mapping*, 31(3):398–409, 2010.
- Xiaojian Kang, Timothy J Herron, Anthony D Cate, E William Yund, and David L Woods. Hemispherically-unified surface maps of human cerebral cortex: reliability and hemispheric asymmetries. *PloS one*, 7(9):e45582, 2012.
- Robert Leech, Rodrigo Braga, and David J Sharp. Echoes of the brain within the posterior cingulate cortex. *The Journal of Neuroscience*, 32(1):215–222, 2012.
- Yonghui Li, Yong Liu, Jun Li, Wen Qin, Kuncheng Li, Chunshui Yu, and Tianzi Jiang. Brain anatomical network and intelligence. *PLoS Comput Biol*, 5(5):e1000395, 2009.

- Sophia Mueller, Danhong Wang, Michael D Fox, B T Thomas Yeo, Jorge Sepulcre, Mert R Sabuncu, Rebecca Shafee, Jie Lu, and Hesheng Liu. Individual variability in functional connectivity architecture of the human brain. *Neuron*, 77(3):586–95, Feb 2013. doi: 10.1016/j.neuron.2012.12.028.
- Krzysztof Nowicki and Tom A. B Snijders. Estimation and prediction for stochastic block-structures. *Journal of the American Statistical Association*, 96(455):1077–1087, Sep 2001. doi: 10.1198/016214501753208735.
- Nicholas G. Polson, James G. Scott, and Jesse Windle. Bayesian inference for logistic models using pólya gamma latent variables. *Journal of the American Statistical Association*, 108(504):1339–1349, Dec 2013. doi: 10.1080/01621459.2013.829001.
- Mikhail Rubinov and Olaf Sporns. Complex network measures of brain connectivity: uses and interpretations. *Neuroimage*, 52(3):1059–1069, 2010.
- Cornelis J Stam. Modern network science of neurological disorders. *Nature Reviews Neuroscience*, 15(10):683–695, 2014.
- Hua Zhou, Lexin Li, and Hongtu Zhu. Tensor regression with applications in neuroimaging data analysis. *Journal of the American Statistical Association*, 108(502):540–552, 2013.